Generation of Patient-specific Structured Hexahedral Mesh of Aortic Aneurysm Wall

Farah Alkhatib, George C. Bourantas, Adam Wittek, and Karol Miller

Abstract Abdominal Aortic Aneurysm (AAA) is an enlargement in the lower part of the main artery "Aorta" by 1.5 times its normal diameter. AAA can cause death if rupture occurs. Elective surgeries are recommended to prevent rupture based on measurement of AAA diameter and diameter growth rate. Reliability of these geometric parameters to predict the AAA rupture risk has been questioned, and biomechanical assessment has been proposed to distinguish between patients with high and low risk of AAA rupture. Stress in aneurysm wall is the main variable of interest in such assessment. Most studies use finite element method to compute AAA stress. This requires discretising patient-specific geometry (aneurysm wall and intraluminal thrombus ILT) into finite elements/meshes. Tetrahedral elements are most commonly used as they can be generated in seemingly automated and effortless way. In practice, however, due to complex aneurysm geometry, the process tends to require time-consuming mesh optimisation to ensure sufficiently high quality of tetrahedral elements. Furthermore, ensuring solution convergence requires large number of tetrahedral elements, which leads to relatively long computation times. In this study, we focus on generation of hexahedral meshes as they are known to provide converged solution for smaller number of elements than tetrahedral meshes. We limit our investigation to already existing algorithms and software packages for mesh generation. Generation of hexahedral meshes for continua with complex/irregular geometry, such as aneurysms, requires analyst interaction. We propose a procedure for generating high quality patient-specific hexahedral discretisation of aneurysm wall using the algorithms available in commercial software package for mesh generation. We demonstrate, for the actual aneurysms, that the procedure facilitates patient-specific mesh generation within timeframe consistent with clinical workflow while requiring only limited input from the analyst.

Keywords Abdominal aortic aneurysm · structured hexahedral elements · Patient-specific aneurysm wall

F. Alkhatib (✉) · G. C. Bourantas · A. Wittek · K. Miller
Intelligent Systems for Medicine Laboratory, The University of Western Australia, Perth, Western Australia, Australia
E-mail: farah.alkhatib@research.uwa.edu.au

K. Miller
Harvard Medical School, Boston, MA, USA

1 Introduction

Abdominal Aortic Aneurysm (AAA) is a permanent and irreversible enlargement in the lower part of the aorta [1], the main artery that pumps blood from the heart to the rest of human body. It is a chronic vascular disease of elderly men (over 65 years old). Prevalence is regarded as negligible before the age of 55 – 60 years [2]. AAA prevalence in women is up to 4 – 6 times less than in men [3].

AAA is usually diagnosed incidentally by unrelated examination as it is symptomless disease [2]. The most fatal event of AAA is rupture, where mortality rate can reach up to 90% [4] leading to 200,000 deaths annually worldwide [5] and around 1,500 deaths yearly in Australia and the Oceania region [6].

According to current AAA management, patients undergo elective surgical intervention if their maximum aortic diameter is more than 55 mm for men and 50 mm for women [7, 8]. Below these recommended thresholds patients are placed on surveillance program that monitors the aneurysm growth rate. The surgery is recommended if the growth rate exceeds 10 mm/year. Australia has a high rate of AAA repairs below these recommended thresholds compared to other Western countries. However, the probability for aneurysms with aortic diameter of 40 – 50 mm under surveillance to rupture is only 0.4% per year, which is lower than the risk of death due to the postoperative complications [2].

This raises the question of how to best manage AAAs as there is a balance between interventions to prevent AAA rupture versus overtreatment that may cause harm to patients and incur non-essential medical cost. Over the last 25 years, researchers introduced different AAA biomechanical rupture risk indicators or indices to identify patients at high risk of AAA rupture [9-13] and conversely those at low risk for whom surgical intervention can be avoided. Evaluation of such indices is beyond the scope of this study. Biomechanical indices for evaluating the AAA rupture risk strongly rely on computation of AAA wall stress [9]. Finite element method (FEM) dominates such computations. It requires discretising patient-specific geometry (aneurysm wall and intraluminal thrombus ILT) into finite elements/meshes as a part of creating the finite element model.

Patient-specific tetrahedral mesh generation is often used in computational biomechanics analysis of AAA as it is believed that such meshes can be created automatically with high element quality by analysts without expertise in computational grid generation [13, 14]. In a study by Miller et al. [15], AAA (aneurysm wall and ILT) finite element models contained more than 1 million tetrahedral elements. This high number of elements ensures convergent solution, but tends to result in relatively long computational times. Furthermore, automated elimination of low quality tetrahedral elements typically requires application of mesh optimisation procedures. From our experience, presence of even small number of low quality elements may lead to unreasonably long optimisation times (up to around 40 – 50 minutes of a personal computer with Intel quad-core i7 processor). Therefore, we focus on hexahedral meshes as they require a smaller number of elements than tetrahedral meshes [16]. For aneurysm walls discretised using 30,000 to 50,000 hexahedral elements, around 500,000 tetrahedral elements were needed to achieve similar geometric discretisation accuracy [17].

Generation of high quality structured (mapped) hexahedral finite element meshes of healthy blood vessel walls can be done automatically by defining the vessels centrelines [18-20] using freely available software such as pyFormex (https://github.com/dladd/pyFormex) and Gmsh (https://gmsh.info/). This, however, does not extend to complex/irregular geometry of AAAs. Generation of structured hexahedral meshes of AAAs tends to require expert's knowledge of finite element meshing procedures and substantial manual effort of the analyst. Specialised mesh generation code developed by Tarjuelo-Gutierrez et al. [21] facilitates construction of hexahedral meshes for aneurysm wall and thrombus including the bifurcations. It relies on connecting the extracted axial and longitudinal lines in the aneurysm from the manual MRI (Magnetic Resonance Imaging) segmentation and the calculated aneurysm centreline. Need for substantial effort of the analyst was also reported in the studies using well established commercial mesh generators. Application of CEM CFD 14.5 (Ansys Inc., USA) to create patient-specific hexahedral finite element meshes of aneurysm wall required 4 – 8 hours of analyst's work per case [12, 22]. Mayr et al. [23] used CUBIT mesh generator (https://cubit.sandia.gov/) to create hexahedral elements for aortic aneurysms to be used in fluid-structure interaction simulation. Distinct advantage of CUBIT that it can automatically partition complex geometries into mappable volumes to build structured hexahedral mesh. CUBIT is available for US government use only. However, its commercial version, Coreform Cubit (https://coreform.com/products/coreform-cubit/free-meshing-software/), has no such restriction. A4Clinics Vascops (http://www.vascops.com/en/vascops-A4clinics.html) software to biomechanically analyse AAA rupture risk creates a hexahedral aneurysm wall with a minimal user interaction. Their meshing algorithm limits any mesh refinement along the circumferential and axial directions of aneurysm wall and ILT, which creates one layer through wall thickness and coarse elements for thick ILT [24]. However, in several studies it has been argued that at least two elements across the AAA wall thickness is needed for converged solution in terms of stress computation [25] . Zhang et al. [16, 26] have successfully created unstructured hexahedral meshes from volumetric data (medical images as an example). Automated unstructured hexahedral elements for aneurysm wall and ILT using Harpoon (http://www.sharc.co.uk/index.htm) was done by Maier et al. [27]. Our experience indicates that unstructured hexahedral meshes may contain some poor quality elements, in particular elements with very low (close to zero or even negative) Jacobian quality measure [26, 28].

In this study, we demonstrate a procedure to create a high quality patient-specific structured hexahedral mesh of aortic aneurysm wall models using commercially available mesh generators for stress computation in the aneurysm wall. We use tetrahedral elements for the intraluminal thrombus (ILT) because of its complex geometry. In addition, accurate ILT stress analysis is not a variable of interest as an indicator of AAA rupture risk, and hence we use tetrahedral elements.

2 Methods

2.1 Patient's data and patient-specific AAA geometry

A contrast-enhanced computed tomography angiography (CTA) image data-set of four abdominal aortic aneurysm (AAA) patients with an average maximum aortic diameter of 55 mm (standard deviation = 9 mm) were used to demonstrate the meshing techniques proposed and used in this work. The CTA images were acquired at Fiona Stanley Hospital (Murdoch, Western Australia, Australia) using SOMATOM Definition Flash CT Scanner (Siemens Healthineers AG, Forchheim, Germany). The spatial resolution (voxel size) of the CTA images is 0.625x0.625x1.5 mm^3. Patients gave their informed consent before acquiring the images according to the Declaration of Helsinki.

The patient-specific AAA geometries were segmented from the CTA images using the open-source medical image analysis package, 3D Slicer (https://www.slicer.org/) [29]. The contrast-enhanced images allowed an automated segmentation for the lumen (blood channel) using the threshold algorithm in 3D Slicer segmentation module. The aneurysm (wall and the intraluminal thrombus 'ILT') needed some manual work to distinguish between the aneurysm and surrounding tissues. Figure 1 shows the segmented patient-specific AAA geometry for a selected case (Patient 1); the blue geometry is the aneurysm wall and the red geometry is the ILT. We assumed constant wall thickness of 1.5 mm for the aneurysm wall, as there is no reliable method to accurately determine AAA wall thickness from CTAs only has developed yet [30].

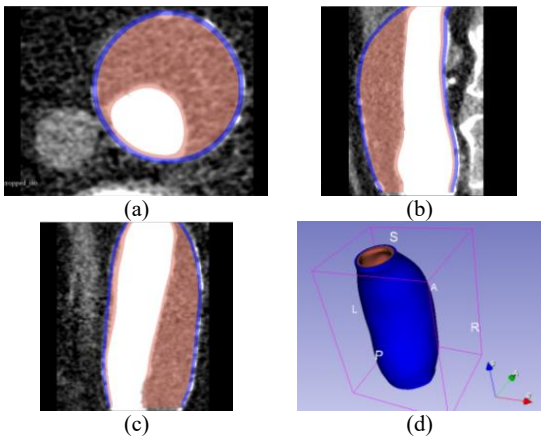

Fig. 1 Patient-specific abdominal aortic aneurysm (AAA) geometry segmented from computed tomography angiography (CTA) using 3D Slicer. The segmented aneurysm wall with constant thickness of 1.5 mm is shown in blue and the segmented intraluminal thrombus (ILT) is shown in red; (a) a slice from the axial view of AAA, (b) a slice from the sagittal view of AAA, (c) a slice from the coronal view of AAA, and (d) the 3D rendered AAA.

2.2 Generation of patient-specific AAA computational grids

2.2.1 Patient-specific AAA meshes

Different meshing tools and algorithms can be used to generate hexahedral elements for the aneurysm wall as stated in Introduction. We initially attempted to use an in-house algorithm (implemented using MATLAB) that reconstructs the aneurysm geometry using the aortic centreline and maximum distances from this centreline to the aortic wall. This algorithm defines subdivided circles and ellipses orthogonal to the centreline ready to be connected using splines to form surface quadrilateral meshes. We faced two main issues in this early-stage algorithm, (1) the circles and ellipses may overlap in the locations that have a large change in wall curvature, and (2) a smoothing technique (Laplace smoothing as an example [31]) should be used to improve the elements shape and mesh quality.

Fully automated hexahedral meshing was not possible for the aneurysm wall using available open-source and commercial mesh generators because of its irregular and asymmetrical shape. We initially used the mesh generator available in ABAQUS/CAE (https://www.3ds.com/products-services/simulia/products/abaqus/) finite element pre-processor. It provides high quality element generation. However, it strongly relies on the user's expertise and requires substantial input (manual mesh generation work) from the user as the AAA geometry needs to be subdivided into many partitions in order to create a structured hexahedral mesh. In this study, we used the industrially applied mesh generation software Altair HyperMesh (https://www.altair.com/hypermesh) to create a high quality hexahedral mesh of AAA wall. Our Intelligent Systems for Medicine Laboratory (ISML) team has many years of experience in using HyperMesh, and HyperMesh can generate high quality meshes from CAD (Computer-Aided Design) or image-defined geometries.

We imported the geometry of AAA wall extracted from the CTA images in STL (Stereo Lithography) format. Because of the irregular geometry of AAA, the geometry had to be partitioned to create the structured (mapped meshing) hexahedral mesh. Figure 2 shows the four aneurysm wall geometries meshed in this study.

The 3D hexahedral mesh (Figure 3a) was created by sweeping the 2D meshed ring (Figure 3b) along the aneurysm wall. The created 2D top ring of quadrilateral elements in the aneurysm wall defines the element size and number of hexahedral layers (elements) through wall thickness. We used two elements (size of 0.75 mm) through the wall thickness.

We created tetrahedral elements for the aneurysm intraluminal thrombus (ILT) using HyperMesh because of its complex shape. The transition between the quadrilateral surface meshes to tetrahedral volume meshes was important to create the shared conformal surface between the hexahedral aneurysm wall and the tetrahedral ILT (Figure 4a). We used the inner wall surface topology (nodes location) to create the outer surface of the ILT (triangular elements). We imported the inner surface of

the ILT (the surface of the lumen segmented in 3D Slicer) and created a dummy mesh to close the top and bottom caps of the ILT (Figure 4b).

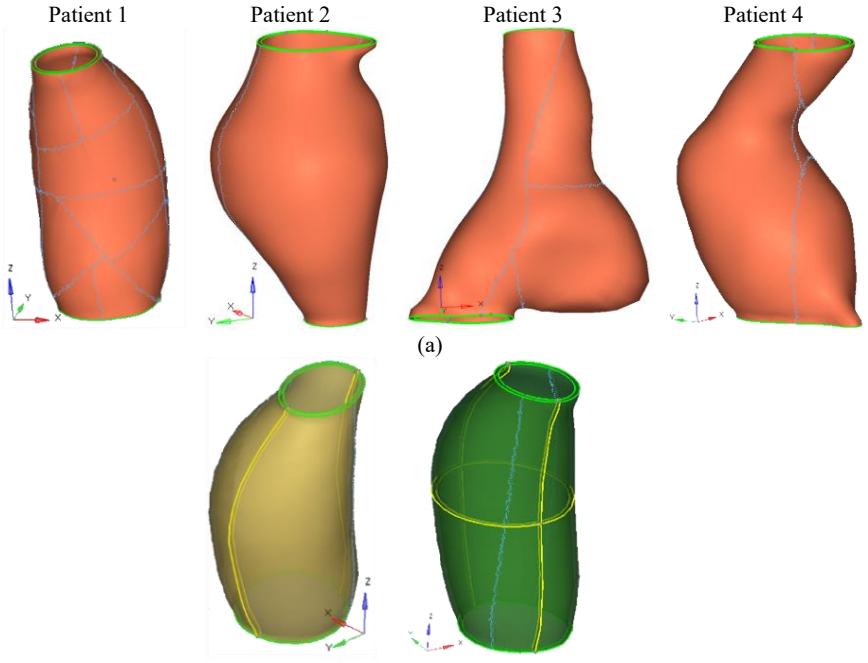

Fig. 2 Aneurysm wall geometries extracted from CTA images and imported in STL format to HyperMesh; (a) geometries of the four patients, orange geometries cannot be meshed directly and at least one partition is needed to create the mapped mesh, (b) partitioned geometry ready for mapped (structured) meshing (Patient 1) using one plane (yellow geometry) or two planes (green geometry), the yellow lines present the planes used as partitions. According to HyperMesh colour code, yellow geometries can be meshed in one direction and green geometries in three directions (from three sides).

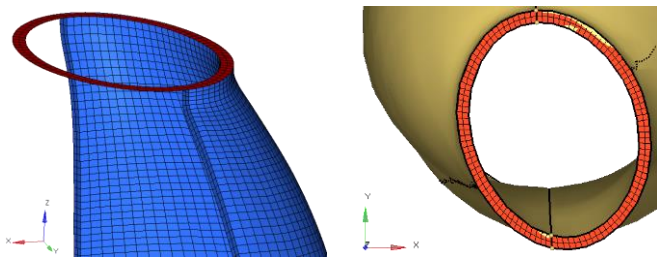

Fig. 3 Hexahedral meshing of aneurysm wall, (a) section of aneurysm wall (blue elements) showing the hexahedral meshes created by sweeping the quadrilateral 2D ring (red elements), and (b) top view of the aneurysm wall geometry that has the generated 2D top ring of quadrilateral elements used to create the 3D volume wall (hexahedral elements), element size is 0.75 mm.

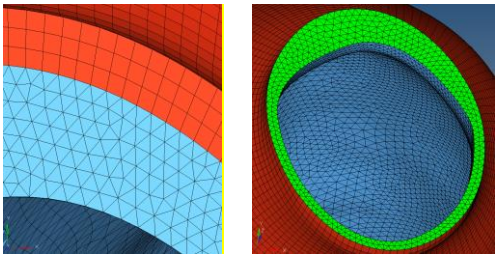

a b

Fig. 4 Generation of tetrahedral intraluminal thrombus (ILT) mesh using HyperMesh. (a) The top view of abdominal aortic aneurysm (AAA) showing the wall in red and ILT in blue, (b) 2D top cap created (green) to close the volume of ILT and generate the tetrahedral mesh.

As the ILT volume is closed, a tetrahedral automated mesh fills this empty volume, allowing the algorithm to reduce number of elements inside ILT, and hence the computation time in the finite element solution is minimised. We kept the existing nodes/locations for both surfaces of wall and ILT, and allowed the splitting of quadrilaterals into triangles to avoid the creation of pyramid elements. The upper and lower caps created (dummy mesh) we set them as freely adjusted nodes. A section view of the tetrahedral ILT created is shown in Figure 5.

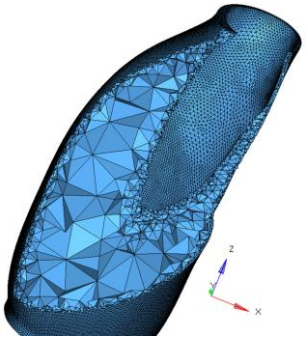

Fig. 5 Meshed tetrahedral intraluminal thrombus (ILT).

2.2.2 Element quality

Hexahedral meshes We used the following two measures to evaluate quality of hexahedral elements: (1) normalised/scaled Jacobian [26, 28] (a Jacobian value of 0.6 and higher is recommended [32]), and (2) the minimum and maximum allowable interior angles of a quadrilateral face (the suggested limits are between 45° and 135° [32]) — see Figure 6a for definition. Both measures need to be used as we found that some elements have high Jacobian, but their maximum or minimum interior angles are out of the recommended range. Figure 6a shows an example of such low quality element. We confirmed that such elements could be avoided by increasing the number of partitions or sections of the AAA geometry and by decreasing the element size.

Tetrahedral meshes We analysed quality of tetrahedral elements using the following two measures: (1) maximum and minimum allowable interior angle for triangles [32], and (2) the volumetric skew [33]:

$$Volumetric\ skew = 1 - \frac{actual\ tetrahedron\ volume}{ideal\ tetrahedron\ volume} \quad (1)$$

Where ideal tetrahedron is an equilateral tetrahedron with the same circumradius of the actual tetrahedron, (i.e. circumradius is radius of a sphere passing through the four vertices of the tetrahedron).

The recommended interior angles range between 30° and 120°. Volumetric skew of 1 means a tetrahedral element degenerated to triangle (Figure 6b). Volumetric skew of 0 means an ideal (equilateral) tetrahedron.

We found that, for both hexahedral and tetrahedral mesh, all poor quality elements were located at the top or bottom (aortic bifurcation) edges of the AAA. These edges are rigidly constrained in the AAA biomechanical models (including the models created and used in this study) [13] and therefore are of limited interest for the AAA stress analysis.

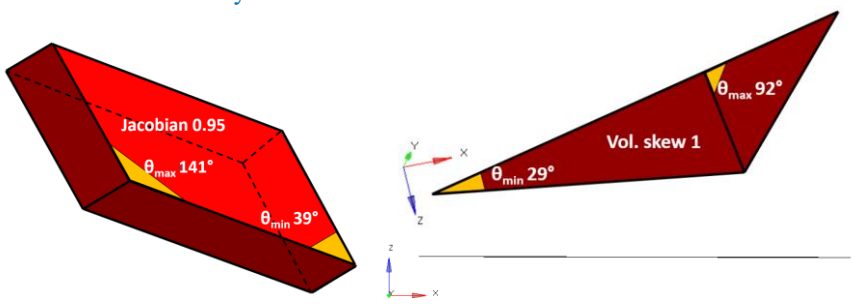

a b

Fig. 6 Examples of low quality elements, (a) hexahedral element with Jacobian of 0.95, but with minimum interior face angle of 39.25° and maximum interior face angle of 141.36° that are out of the recommended allowable angles (45° - 135°) [32]. Interior angles are highlighted in yellow, and (b) two views showing a tetrahedral element with volumetric skew of 1 which means a "flat" tetrahedral element degenerated to triangle.

2.3 Stress computation in AAA wall

Following our previous studies [13, 34], we used linear static finite element analysis implemented in ABAQUS/Standard finite element code [35] (https://www.3ds.com/products-services/simulia/products/abaqus/) to calculate the AAA wall stress. This approach has been used in the freely available open-source software platform *BioPARR – Biomechanics based Prediction of Aneurysm Rupture Risk* (https://bioparr.mech.uwa.edu.au/) for biomechanical analysis of AAA [13]. It relies on the observation that as patient images show the deformed (due to loading by the blood pressure) AAA geometry, the internal forces on the blood vessel wall that balance the applied pressure can be calculated from the principles of statics [13,

34]. This implies that if the computational biomechanics simulations are set-up in such a way that the deformed AAA geometry remains unchanged when loaded by blood pressure, one should obtain the stress field in the AAA wall that balances the pressure [34]. Such field is for practical purposes independent of the material properties of aorta tissue if the material is homogenous [34, 36].

For both aortic wall and ILT, we used nearly incompressible (Poisson's ratio of 0.49) linear elastic material model. Following [15], the ILT was defined as 20 times more compliant than the AAA wall. To construct hexahedral meshes, we used hybrid 20-noded quadratic hexahedral element with reduced integration (8 integration points), — element C3D20RH in ABAQUS finite element code. For tetrahedral meshes, we used hybrid 10-noded quadratic tetrahedral element — element C3D10H in ABAQUS finite element codes. Application of hybrid formulation prevents volumetric locking for the nearly incompressible materials we used.

The aneurysm was uniformly loaded at the internal surface of the ILT by the patient-specific blood pressure measured 5 minutes before acquiring the CT images [12, 37, 38]. We used mean arterial blood pressure (MAP) that is calculated from the systolic and diastolic pressures (MAP = 1/3 systolic pressure + 2/3 diastolic pressure). The aneurysm was fully supported at its top and bottom edges.

We analysed the maximum principal stress of the patient-specific aneurysm walls as it provides indication of the internal forces in the aorta that balance the blood pressure [13]. The residual stresses of the aorta were not taken into account in this study as we focus on the method of generating high quality hexahedral meshes for aneurysm wall rather than the AAA rupture assessment through stress computation.

We compared the contours of the maximum principal stress and distribution of the 99^{th} percentile of the maximum principal stress in the aneurysm wall obtained using the hexahedral and tetrahedral finite meshes. We used 99^{th} percentile rather the peak values to eliminate the artefacts and uncertainties due to the AAA segmentation and AAA geometry discretisation when generating the finite element meshes [39].

3 Results

3.1 Computational grid (finite element mesh) convergence

We performed a mesh convergence study on one of the analysed AAAs (Patient 1) to ensure that computation of stress in aneurysm wall is independent of mesh size while reducing computational time. We created three hexahedral aneurysm wall models. The first model included 2 layers of hexahedral elements through wall thickness, the second model had 3 layers while the third model had 4 layers. We calculated the maximum principal stress in those three models using

ABAQUS/Standard on Intel(R) Core(TM) i7-5930K CPU @ 3.50 GHz with 64.0 GB of RAM running Windows 8 OS. The finite element models used when analysing the mesh convergence did not include the ILT. The inner surface of the AAA wall was loaded with 12 kPa (MAP, mean arterial pressure for Patient 1).

Table 1 summarises the mesh characteristics of each studied finite element model. It also includes the peak and 99th percentile values of maximum principal stress for the three models. The peak stress values typically occur at the fixed (rigidly constrained) nodes of the top and bottom edges of the aneurysm wall, which can be regarded as a modelling artefact. Therefore, we compared 99th percentile of the maximum principal stress.

Table 1 Mesh characteristics, maximum principal stress values (peak and 99th percentile), and finite element models computation time for the studied models.

	Model 1	**Model 2**	**Model 3**
No. of hexahedral elements through wall thickness	2	3	4
Element size (mm)	0.75	0.5	0.375
No. of elements	27,972	95,190	225,676
No. of nodes	154,734	477,787	1,075,083
Peak of maximum principal stress (MPa)	0.5300	0.6070	0.6831
99th percentile of maximum principal stress (MPa)	0.2700	0.2620	0.2557
Computation time (sec)	23	103	568

Figure 7 shows the maximum principal stress for the three studied models with respect of a percentile rank of the stress values. We refer to Figure 7 as the maximum principal stress percentile plot. As for all three models, the maximum principal stress percentile plots are very close.

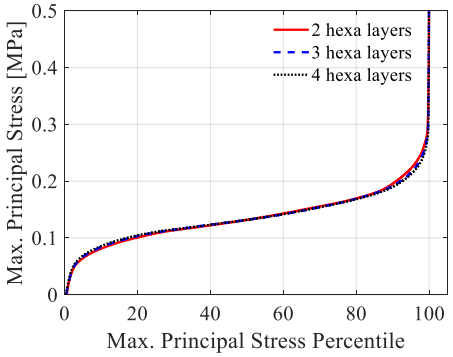

Fig. 7 Maximum principal stress percentile plot for the three studied models to show the mesh independency for stress calculations.

We selected four nodes in the three aneurysm wall models to compare the maximum principal stress. The selected nodes were in the middle of the aneurysm wall, two of them were on the outer surface of the wall and two on the inner surface (Figure 8a). The four nodes had the same location/coordinates for all three studied

aneurysm wall models. Figure 8b shows convergence of the computed stress at the 4 selected nodes. We conclude that two layers of hexahedral elements through the aneurysm wall thickness are sufficient to ensure converged stress computation.

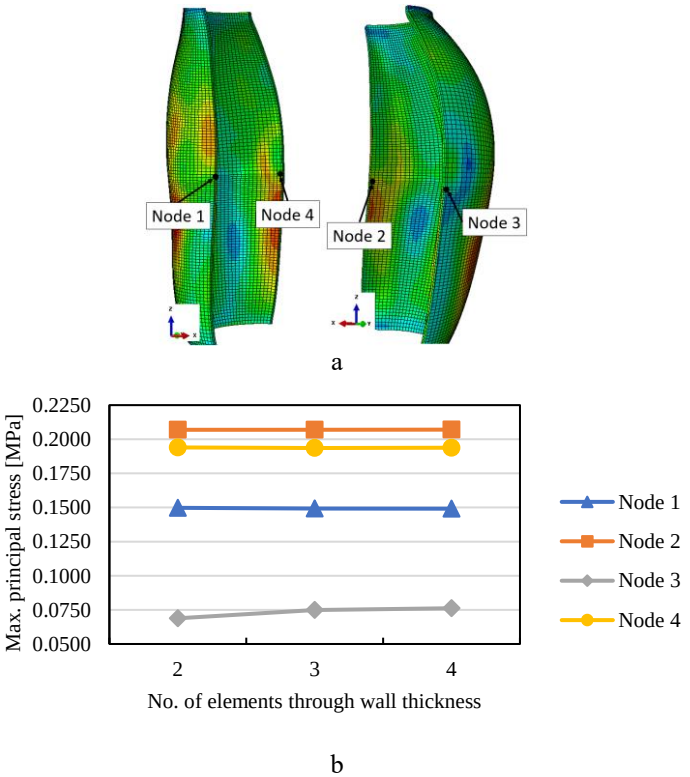

Fig. 7 (a) Location of the four selected nodes used to analyse convergence of computing the maximum principal stress in the aneurysm wall; and (b) convergence analysis of the computation of the maximum principal stress in the aneurysm wall when varying the number of elements through the wall.

3.2 Computational grids and element quality

The created computational grids (hexahedral finite element meshes) for four patient analyses in this study are shown in Figure 9. These meshes were generated using two hexahedral elements through wall thickness and element size of 0.75 mm.

Table 2 reports the number of low quality elements according to the quality measures used, Jacobian and minimum/maximum interior allowable angles for hexahedral elements, and volumetric skew and minimum/maximum interior allowable angles for tetrahedral elements. We noticed that low quality tetrahedral elements in AAA are located at the top and bottom edges of the aneurysm model, where the

aneurysm is fully supported. They account for a very small fraction (less than 0.02% of the total number of elements in the AAA model).

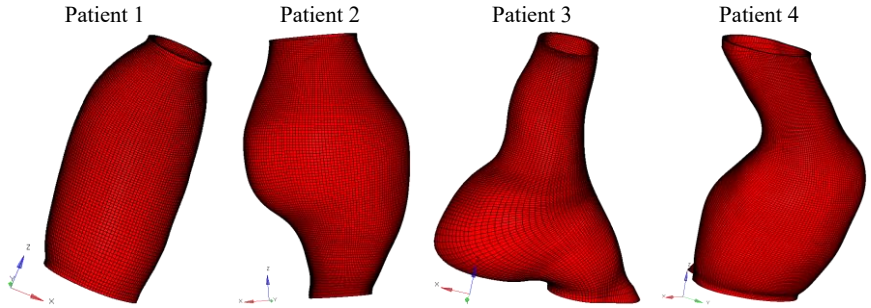

Fig. 9 Hexahedral meshes of the aneurysm wall created using HyperMesh with an element size of 0.75 mm.

Table 2 Summary of low quality elements according to the used quality measures for the AAA wall (hexahedral mesh) and ILT (tetrahedral elements) models for four AAA patients analysed in this study.

	Patient 1		**Patient 2**		**Patient 3**		**Patient 4**	
Part	Wall	ILT	Wall	ILT	Wall	ILT	Wall	ILT
No. of elements	21,090	290,924	35,616	180,162	27,072	90,571	46,472	234,976
No. of nodes	116,883	251,506	197,160	309,160	149,648	168,802	256,780	391,362
No. of elements failed to Jacobian	0	N/A	0	N/A	5	N/A	0	N/A
Min. Jacobian	0.86	N/A	0.73	N/A	0.57	N/A	0.72	N/A
No. of elements failed to volumetric skew	N/A	3	N/A	0	N/A	84	N/A	147
Max. vol. skew	N/A	1	N/A	0.93	N/A	1	N/A	1
No. of elements failed to min/max angle	0	41	4	37	67	105	50	163
Min angle	50°	0.5°	45°	9°	26°	6°	37°	5°
Max angle	131°	179°	140°	136°	162°	155°	146°	160°

N/A: not applicable measure for the specific case.

3.3 Aneurysm wall stress

Figure 10 shows the maximum principal stress contour plots for the aneurysms analysed in this study. Table 3 compares the peak and 99th percentile of maximum

principal stress for the hexahedral and tetrahedral meshes of the aneurysm wall. There are only minor differences between the results obtained using hexahedral and tetrahedral meshes. However, the number of elements (over 1 million) in tetrahedral meshes is appreciably larger than in hexahedral meshes (around 35,000 elements). Consequently, more than fivefold reduction in computation time is observed for the models using hexahedral meshes. The finite element models computation time for both grids is reported using Intel(R) Core(TM) i7-5930K CPU @ 3.50 GHz with 64.0 GB of RAM running Windows 8 OS. Patient 4 model using hexahedral elements for the aneurysm wall computation time was higher than the tetrahedral elements for the same aneurysm wall as this model has relatively huge ILT, ILT was discretised using tetrahedral meshes in both models.

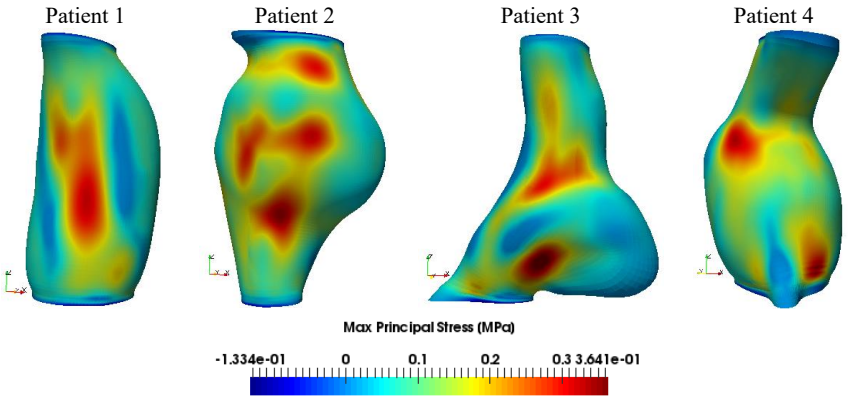

Fig. 10 Maximum principal stress contour plots in the studied hexahedral meshes of aneurysm walls from the finite element solution.

Table 3 Comparison of the peak values and 99th percentile of the maximum principal stress obtained using hexahedral and tetrahedral meshes for the four aneurysms analysed in this study. All simulations were conducted using a computer with Intel(R) Core(TM) i7-5930K CPU @ 3.50 GHz processor and 64.0 GB of RAM running Windows 8 OS.

		Patient 1	**Patient 2**	**Patient 3**	**Patient 4**
Applied pressure/load (kPa)		12	13	13	14
Peak of max. principal stress (MPa)	Hexahedral meshed wall	0.3641	0.4543	0.4383	0.5048
	Tetrahedral meshed wall	0.3880	0.3953	0.4755	0.6074
	Absolute difference	0.0239	0.0590	0.0372	0.1026
99th percentile max. principal stress (MPa)	Hexahedral meshed wall	0.2310	0.2859	0.3037	0.2437
	Tetrahedral meshed wall	0.2034	0.2554	0.2487	0.2176
	Absolute difference	0.0276	0.0305	0.0550	0.0261
Computation time (sec)	Hexahedral meshed wall	157	296	133	1355
	Tetrahedral meshed wall	880	1641	1196	1058

4 Discussion

Hexahedral meshing of aneurysm wall is not a trivial and straightforward problem. In this study, we present a procedure to build hexahedral mesh of abdominal aortic aneurysm (AAA) wall using commercial (industrially applied) HyperMesh mesh generator. The procedure requires 20 – 30 minutes of analyst's time to create a high quality patient-specific mesh of the AAA wall. In future, these steps can be scripted using the language used by HyperMesh with minimum user-intervention. Low quality hexahedral elements could not be completely avoided (see Table 2, Patients 3 and 4) because of complex and irregular geometry of AAAs. However, the number of such elements did not exceed 0.2% of the total number of hexahedral elements in the patient-specific AAA model. From the results obtained in this study, it can be concluded that mesh refinement (increasing the number of elements) could further improve the mesh quality. This, however, increases the computation time with only a negligible change in computed stress. Therefore, we conclude that two hexahedral elements through wall thickness are sufficient to ensure convergence of stress computation.

We were also able to create high quality hexahedral meshes (minimum Jacobian of 0.71) of AAA wall using ABAQUS/CAE mesh generator (see 2.2.1). Although from Figure 11 the mesh density mismatch was obvious because of the inflexibility of defining partition planes in ABAQUS/CAE. Maximum principal stress contour plots and peak values of the maximum principal stress showed very good agreement for the models using the hexahedral meshes created using ABAQUS/CAE meshing tool and HyperMesh. The difference in the peak value of maximum principal stress between these models was only up to 0.0479 MPa. However, HyperMesh required less partitioning (and less analyst's time) than ABAQUS/CAE meshing tool to create mapped hexahedral meshes.

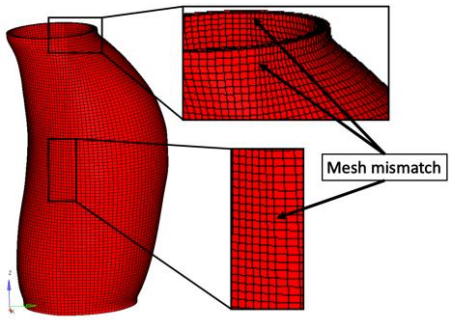

Fig. 11 Hexahedral mesh of the abdominal aortic aneurysm AAA wall generated using ABAQUS/CAE meshing tool.

Acknowledgments The authors acknowledge funding of the Australian Government through the National Health and Medical Research Council NHMRC Ideas Grant, Ideas grant no. APP2001689. This research was carried out while the first author F. A. was in receipt of an "Australian Government Research Training Program Scholarship at The University of Western Australia". The first author acknowledges the support of Ms. Giuliana D'Aulerio of the University of Western Australia Medical School/ Division of Surgery for her contribution in obtaining the ethics

approval. Contributions of Christopher Wood and Jane Polce, radiologists at Medical Imaging Department, Fiona Stanley Hospital (Western Australia) in patient (abdominal aortic aneurysm) CT image acquisition are gratefully acknowledged. We also thank Fiona Stanley Hospital, Perth, Western Australia for providing the patient CT images.

References

[1] Johnston, K. W., Rutherford, R. B., Tilson, M. D., Shah, D. M., Hollier, L., and Stanley, J. C., 1991, "Suggested standards for reporting on arterial aneurysms," Journal of vascular surgery, 13(3), pp. 452-458.
[2] Wanhainen, A., Verzini, F., Van Herzeele, I., Allaire, E., Bown, M., Cohnert, T., Dick, F., van Herwaarden, J., Karkos, C., and Koelemay, M., 2019, "Editor's choice–european society for vascular surgery (ESVS) 2019 clinical practice guidelines on the management of abdominal aorto-iliac Artery aneurysms," European Journal of Vascular and Endovascular Surgery, 57(1), pp. 8-93.
[3] Martufi, G., and Gasser, T. C., 2013, "the role of biomechanical modeling in the rupture risk assessment for abdominal aortic aneurysms," Journal of biomechanical engineering, 135(2), p. 021010.
[4] Upchurch, G. R., and Schaub, T. A., 2006, "Abdominal aortic aneurysm," Am Fam Physician, 73(7), pp. 1198-1204.
[5] Abubakar, I., Tillmann, T., and Banerjee, A., 2015, "Global, regional, and national age-sex specific all-cause and cause-specific mortality for 240 causes of death, 1990-2013: a systematic analysis for the Global Burden of Disease Study 2013," Lancet, 385(9963), pp. 117-171.
[6] Lancet-2017, "The lancet, Global Burden of Disease," https://www.thelancet.com/gbd/gbd-compare-visualisation.
[7] Scott, R., and Group, M. A. S. S., 2002, "The Multicentre Aneurysm Screening Study (MASS) into the effect of abdominal aortic aneurysm screening on mortality in men: a randomised controlled trial," The Lancet, 360(9345), pp. 1531-1539.
[8] Powell, J. T., and Brady, A. R., 2004, "Detection, management, and prospects for the medical treatment of small abdominal aortic aneurysms," Arteriosclerosis, thrombosis, and vascular biology, 24(2), pp. 241-245.
[9] Geest, J. V., Di Martino, E., Bohra, A., Makaroun, M. S., and Vorp, D. A., 2006, "A biomechanics-based rupture potential index for abdominal aortic aneurysm risk assessment: demonstrative application," Annals of the New York Academy of Sciences, 1085, pp. 11-21.
[10] Gasser, T. C., Auer, M., Labruto, F., Swedenborg, J., and Roy, J., 2010, "Biomechanical rupture risk assessment of abdominal aortic aneurysms: model complexity versus predictability of finite element simulations," European Journal of Vascular and Endovascular Surgery, 40(2), pp. 176-185.
[11] Gasser, T. C., Nchimi, A., Swedenborg, J., Roy, J., Sakalihasan, N., Böckler, D., and Hyhlik-Dürr, A., 2014, "A novel strategy to translate the biomechanical rupture risk of abdominal aortic aneurysms to their equivalent diameter risk: method and retrospective validation," European Journal of Vascular and Endovascular Surgery, 47(3), pp. 288-295.
[12] Polzer, S., and Gasser, T. C., 2015, "Biomechanical rupture risk assessment of abdominal aortic aneurysms based on a novel probabilistic rupture risk index," Journal of The Royal Society Interface, 12(113), p. 20150852.
[13] Joldes, G. R., Miller, K., Wittek, A., Forsythe, R. O., Newby, D. E., and Doyle, B. J., 2017, "BioPARR: A software system for estimating the rupture potential index for abdominal aortic aneurysms," Scientific reports, 7(1), p. 4641.
[14] Raut, S. S., Liu, P., and Finol, E. A., 2015, "An approach for patient-specific multi-domain vascular mesh generation featuring spatially varying wall thickness modeling," Journal of biomechanics, 48(10), pp. 1972-1981.
[15] Miller, K., Mufty, H., Catlin, A., Rogers, C., Saunders, B., Sciarrone, R., Fourneau, I., Meuris, B., Tavner, A., and Joldes, G. R., 2020, "Is There a Relationship Between Stress in Walls of Abdominal Aortic Aneurysm and Symptoms?," Journal of Surgical Research, 252, pp. 37-46.
[16] Jessica, Z. Y., 2018, "Image-Based Quadrilateral and Hexahedral Meshing," Geometric Modeling and Mesh Generation from Scanned Images, pp. 193-228.

[17] Wittek, A., Alkhatib, F., Vitásek, R., Polzer, S., and Miller, K., 2022, "On stress in abdominal aortic aneurysm: Linear versus non-linear analysis and aneurysm rupture risk," International Journal for Numerical Methods in Biomedical Engineering, 38(2), p. e3554.
[18] De Santis, G., Mortier, P., De Beule, M., Segers, P., Verdonck, P., and Verhegghe, B., 2010, "Patient-specific computational fluid dynamics: structured mesh generation from coronary angiography," Medical & biological engineering & computing, 48(4), pp. 371-380.
[19] Trachet, B., Renard, M., De Santis, G., Staelens, S., De Backer, J., Antiga, L., Loeys, B., and Segers, P., 2011, "An integrated framework to quantitatively link mouse-specific hemodynamics to aneurysm formation in angiotensin II-infused ApoE−/− mice," Annals of biomedical engineering, 39(9), pp. 2430-2444.
[20] Marchandise, E., Geuzaine, C., and Remacle, J.-F., 2013, "Cardiovascular and lung mesh generation based on centerlines," International journal for numerical methods in biomedical engineering, 29(6), pp. 665-682.
[21] Tarjuelo-Gutierrez, J., Rodriguez-Vila, B., Pierce, D. M., Fastl, T. E., Verbrugghe, P., Fourneau, I., Maleux, G., Herijgers, P., Holzapfel, G. A., and Gómez, E. J., 2014, "High-quality conforming hexahedral meshes of patient-specific abdominal aortic aneurysms including their intraluminal thrombi," Medical & biological engineering & computing, 52(2), pp. 159-168.
[22] Joldes, G. R., Noble, C., Polzer, S., Taylor, Z. A., Wittek, A., and Miller, K., 2018, "A simple method of incorporating the effect of the Uniform Stress Hypothesis in arterial wall stress computations," Acta of Bioengineering and Biomechanics,, 20(3), pp. 59-67.
[23] Mayr, M., Wall, W. A., and Gee, M. W., 2018, "Adaptive time stepping for fluid-structure interaction solvers," Finite Elements in Analysis and Design, 141, pp. 55-69.
[24] Auer, M., and Gasser, T. C., 2010, "Reconstruction and finite element mesh generation of abdominal aortic aneurysms from computerized tomography angiography data with minimal user interactions," IEEE transactions on medical imaging, 29(4), pp. 1022-1028.
[25] Polzer, S., Bursa, J., Gasser, T. C., Staffa, R., and Vlachovsky, R., 2013, "A numerical implementation to predict residual strains from the homogeneous stress hypothesis with application to abdominal aortic aneurysms," Annals of biomedical engineering, 41(7), pp. 1516-1527.
[26] Zhang, Y., and Bajaj, C., 2006, "Adaptive and quality quadrilateral/hexahedral meshing from volumetric data," Computer methods in applied mechanics and engineering, 195(9-12), pp. 942-960.
[27] Maier, A., Gee, M., Reeps, C., Pongratz, J., Eckstein, H.-H., and Wall, W., 2010, "A comparison of diameter, wall stress, and rupture potential index for abdominal aortic aneurysm rupture risk prediction," Annals of biomedical engineering, 38(10), pp. 3124-3134.
[28] Ito, Y., Shih, A. M., and Soni, B. K., 2009, "Octree-based reasonable-quality hexahedral mesh generation using a new set of refinement templates," International Journal for Numerical Methods in Engineering, 77(13), pp. 1809-1833.
[29] Fedorov, A., Beichel, R., Kalpathy-Cramer, J., Finet, J., Fillion-Robin, J.-C., Pujol, S., Bauer, C., Jennings, D., Fennessy, F., and Sonka, M., 2012, "3D Slicer as an image computing platform for the Quantitative Imaging Network," Magnetic resonance imaging, 30(9), pp. 1323-1341.
[30] Andy T. Huynh, K. M., 2022, "Towards accurate measurement of abdominal aortic aneurysm wall thickness from CT and MRI," Computational Biomechanics for Medicine - Towards translation and better patient outcomes, Springer International Publishing.
[31] Bern, M. W., and Plassmann, P. E., 2000, "Mesh Generation," Handbook of computational geometry, 38.
[32] Yang, K.-H., 2017, Basic finite element method as applied to injury biomechanics, Academic Press.
[33] AltairEngineering, 2022, " Altair HyperMesh," https://2022.help.altair.com/2022.1/hwdesktop/hm/topics/chapter_heads/tutorials_r.htm.
[34] Joldes, G. R., Miller, K., Wittek, A., and Doyle, B., 2016, "A simple, effective and clinically applicable method to compute abdominal aortic aneurysm wall stress," Journal of the Mechanical Behavior of Biomedical Materials,, 58, pp. 139-148.
[35] Smith, M., 2009, "ABAQUS/Standard User's Manual, Version 6.9," Providence, RI: Simulia.
[36] Lu, J., Zhou, X., and Raghavan, M. L., 2007, "Inverse elastostatic stress analysis in pre-deformed biological structures: demonstration using abdominal aortic aneurysms," Journal of biomechanics, 40(3), pp. 693-696.
[37] Inzoli, F., Boschetti, F., Zappa, M., Longo, T., and Fumero, R., 1993, "Biomechanical factors in abdominal aortic aneurysm rupture," European journal of vascular surgery, 7(6), pp. 667-674.

[38] Vorp, D. A., Mandarino, W. A., Webster, M. W., and Gorcsan Iii, J., 1996, "Potential influence of intraluminal thrombus on abdominal aortic aneurysm as assessed by a new non-invasive method," Cardiovascular Surgery, 4(6), pp. 732-739.
[39] Speelman, L., Bosboom, E. M. H., Schurink, G. W. H., Hellenthal, F., Buth, J., Breeuwer, M., Jacobs, M. J., and van de Vosse, F. N., 2008, "Patient-specific AAA wall stress analysis: 99-percentile versus peak stress," European Journal of Vascular and Endovascular Surgery, 36(6), pp. 668-676.